Supplementary information

Heterogeneous Warming Rates and Decline in Snow Persistence across Mountains Worldwide

Blau et al

This PDF file includes:

Extended Methods
Figures S1 to S5
Table S1 to S3

Supplementary Methods

To further highlight the relation between snow cover and shortwave radiation, we calculated the surface albedo (α) by dividing outgoing shortwave radiation by incoming shortwave radiation

$$\alpha = \frac{S^{\uparrow}}{S^{\downarrow}}$$

Figure S1: Spatial map of mean state snow cover

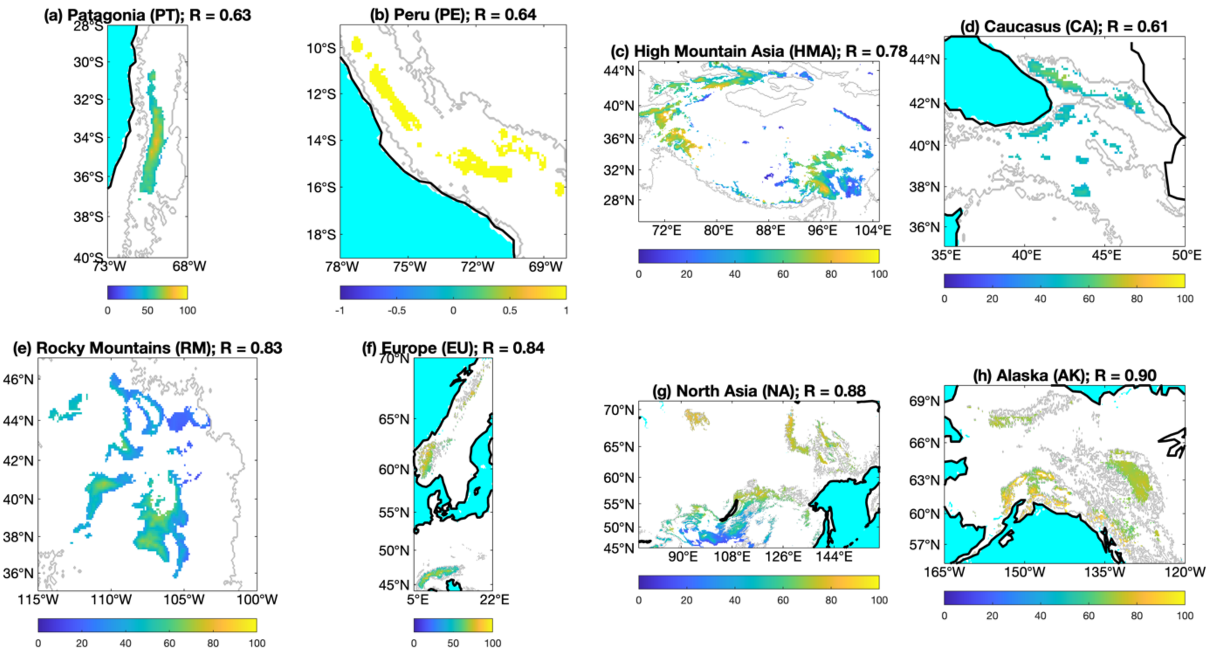

ERA5 snow persistence mean state in each regional box. Shown are only grid points considered in the analysis. The coordinates of the box extent are listed in Table S1.

Figure S2: Data comparison in overlapping periods

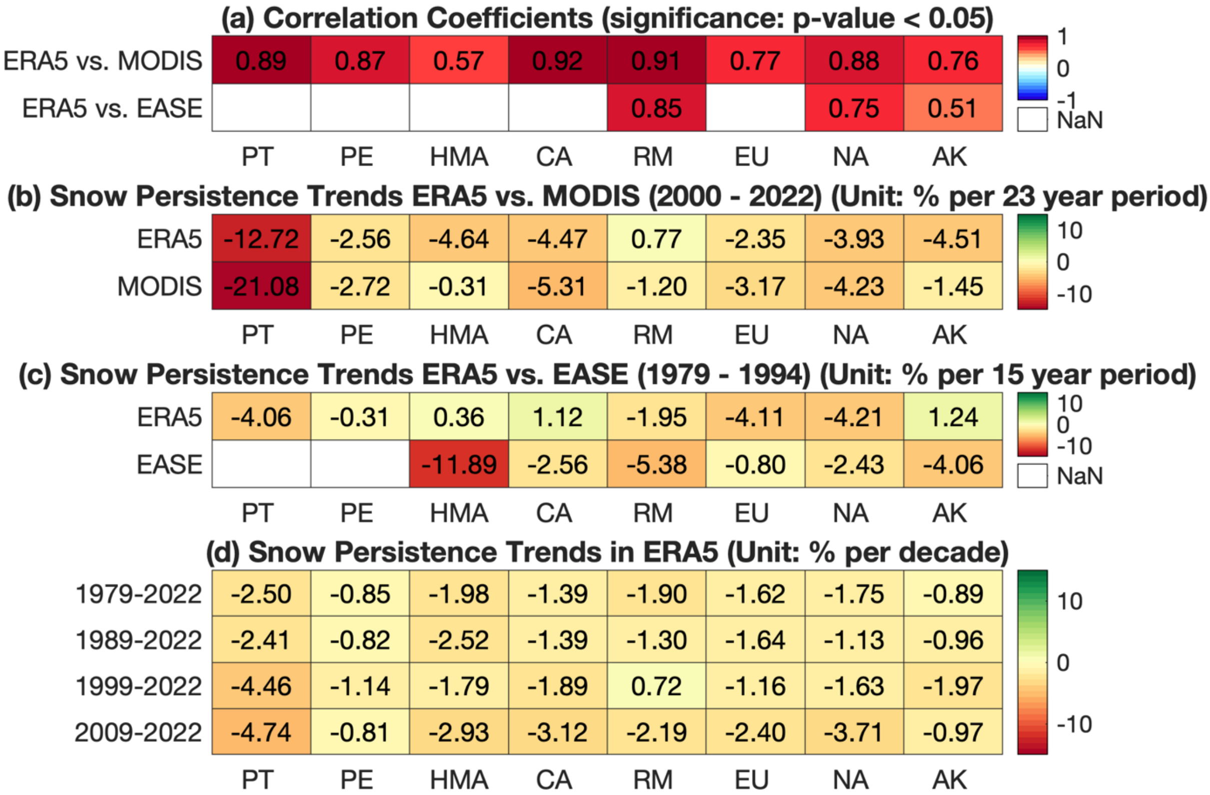

Heat maps of correlation coefficients and trends between ERA5, MODIS and EASE snow persistence time series in overlapping periods – ERA5 and EASE: 1979–1994; ERA5 and MODIS: 2000–2021. (a) shows significant correlation coefficients (0.95 significance level). The other panels show the compares the magnitude of trends between ERA5 and MODIS (b), ERA5 and EASE (c), and two different period of ERA5 data from 1979–1999 and from 2000–2021 (d).

Figure S3: Validation of trends in CMIP6

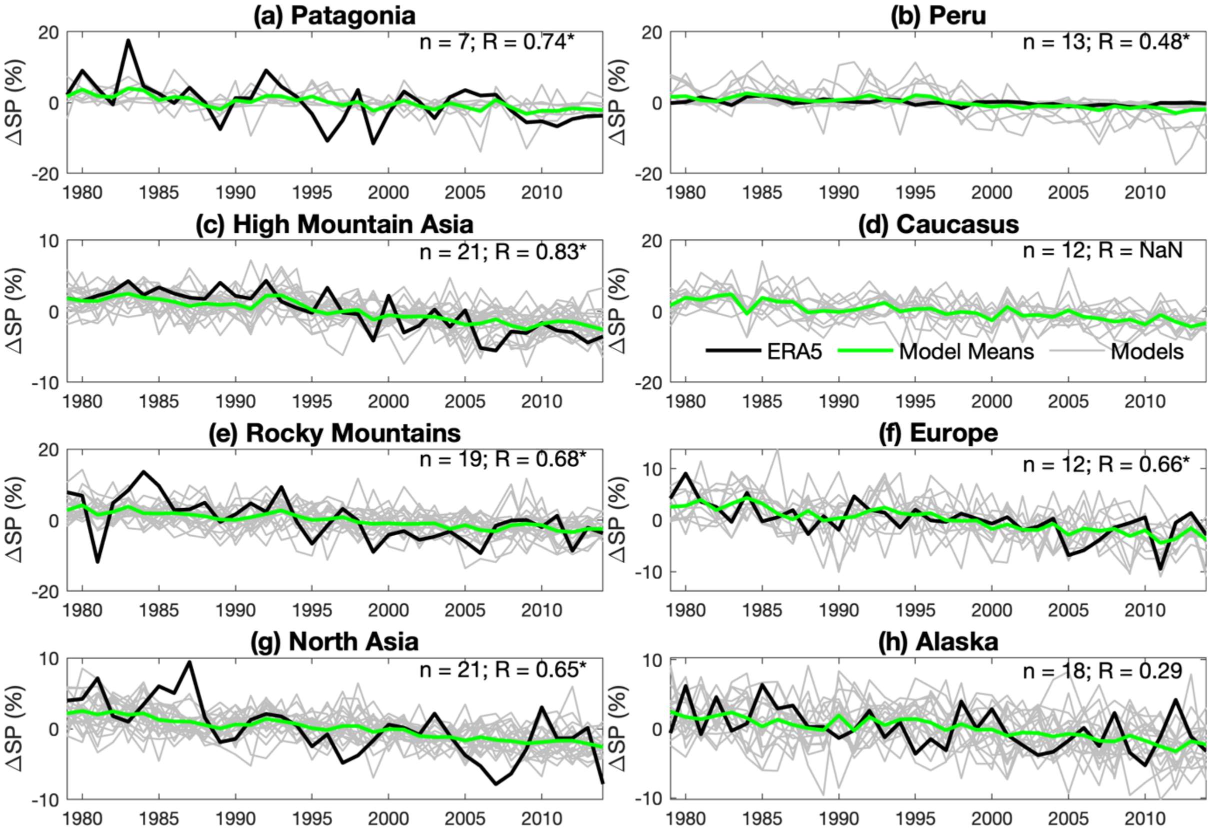

The anomaly timeseries of the ERA5 snow persistence (black line) averaged over the regions is plotted against the model output of the CMIP6 models interpolated on a 1x1° grid for the multi-model mean (green line) and the individual models (gray lines). The numerical in the top right illustrate the numbers models which exhibit mountain snow cover according to the snow cover conditions and the correlation between multi-model mean and ERA5.

Figure S4: CMIP6 Evaluation

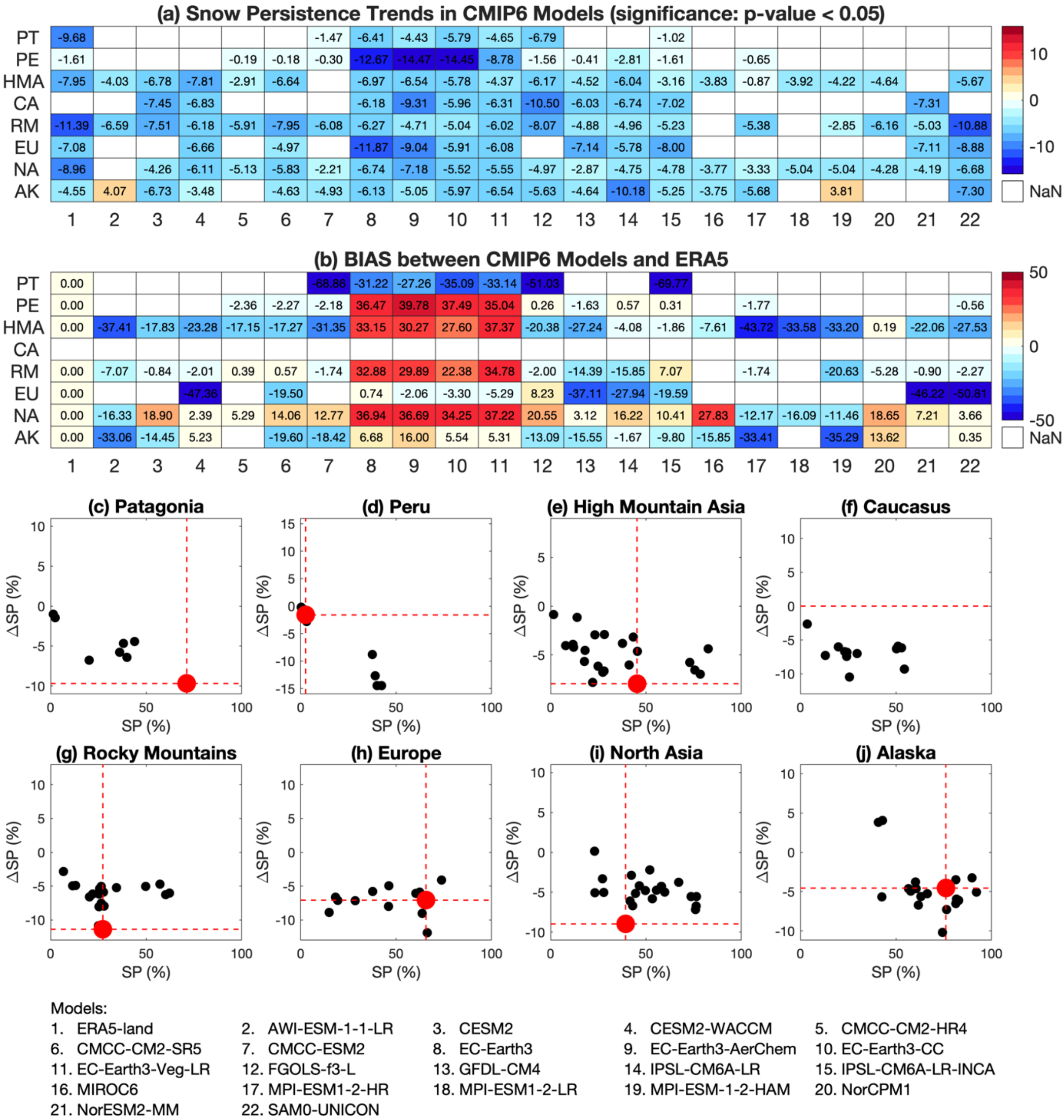

The output of 21 CMIP6 models are compared to ERA5. The trends of ERA5 and the CMIP6 output (a) and the BIAS (b) is shown for each snow mountain region. The scatter plot compares the mean value (y-axis) and trend (x-axis) for each region (c) to (j). The red points denote the ERA5 values, the black dots indicate the result for the different models.

Figure S5: Correlation map

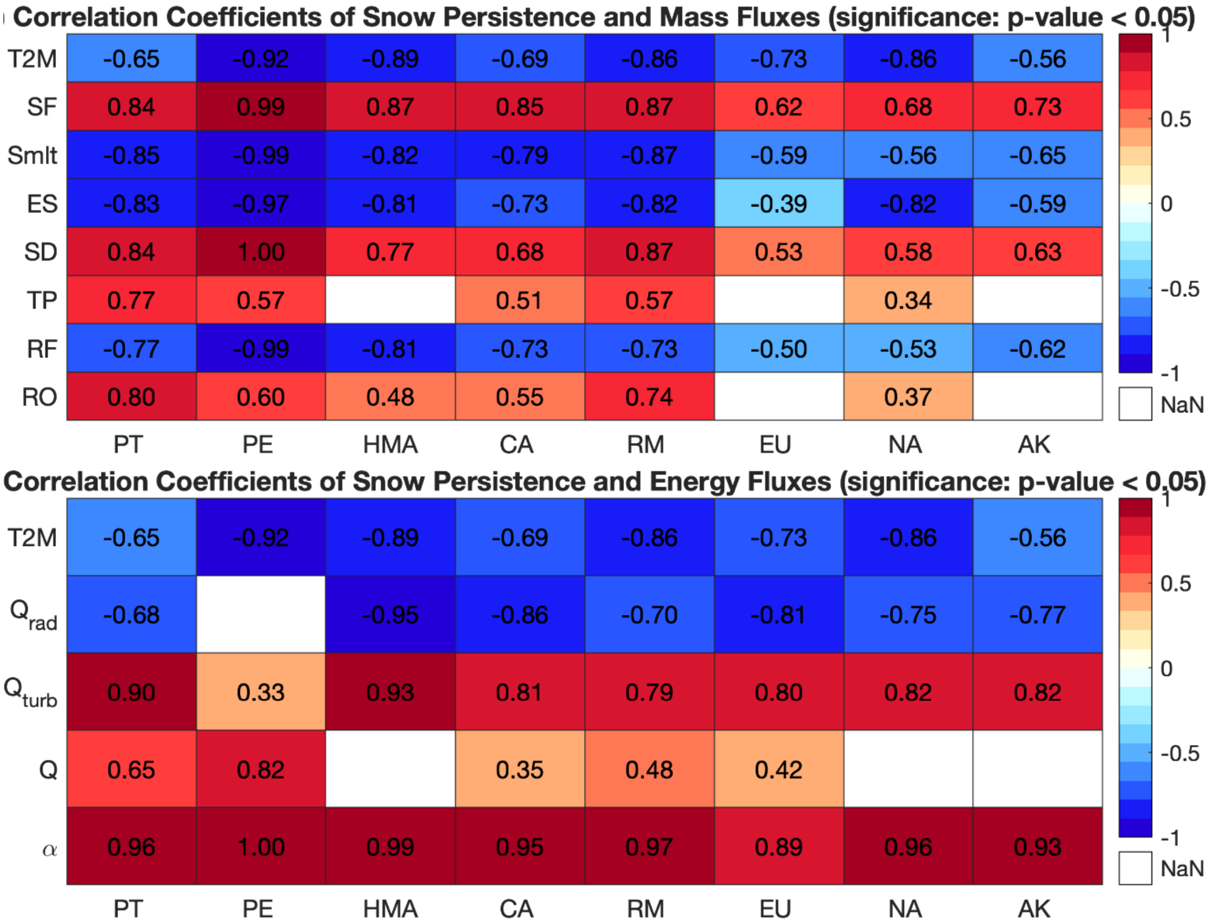

Correlation between snow persistence and (a) different mass fluxes and (b) energy fluxes Only significant correlation coefficients are shown (95 % significance level).

Table S1: Coordinates of regional boxes of considered snow-covered mountains in main Fig 1.

	Region	Coordinates (latitude; longitude)
a	Patagonia (PT)	-40 °N to -28 °N; -73 °E to -68 °E
b	Peru (PE)	-19 °N to -9 °N; -78 °E to -68 °E
c	High Mountain Asia (HMA)	25 °N to 45 °N; 68 °E to 105 °E
d	Caucasus (CA)	35 °N to 45 °N; 35 °E to 50 °E
e	Rocky Mountains (RM)	35 °N to 46 °N; -115 °E to -100 °E
f	Europe (EU)	44 °N to 70 °N; 5 °E to 22 °E
g	North Asia (NA)	45 °N to 71 °N; 75 °E to 160 °E
h	Alaska (AK)	55 °N to 70 °N; -165 °E to -120 °E

Table S2: Comparison of trend magnitude between ERA5, EASE, and MODIS snow persistence data.

	ERA5				ERA5	MODIS	ERA5	EASE
Period	1979–2022	1989–1999	1999–2022	2009-2022	2000–2022		1979-1994	
Time Integration	10 Years				23 Years		15 Years	
PT	-2.50	-2.41	-4.46	-4.74	-12.72	-21.08	-4.06	-
PE	-0.85	-0.82	-1.14	-0.81	-2.56	-2.72	-0.31	-
HMA	-1.98	-2.52	-1.79	-2.93	-4.64	-0.31	0.36	-11.89
CA	-1.39	-1.39	-1.89	-3.12	-4.47	-5.31	1.12	-2.56
RM	-1.90	-1.30	0.72	-2.19	0.77	-1.20	-1.95	-5.38
EU	-1.62	-1.64	-1.16	-2.40	-2.35	-3.17	-4.11	-0.80
NA	-1.75	-1.13	-1.63	-3.71	-4.21	-2.43	-4.21	-2.43
AK	-0.89	-0.96	-1.97	-0.97	-4.51	-1.45	1.24	-4.06

Table S3: List of CMIP6 models including their affiliated research institute and spatial resolution. Of each model the first realization (r1i1p1f1) of the historical run was used. All listed models provided snow cover (snc) and orographic (orog) information.

Model	Research Institute	Spatial Resolution Lon x Lat	References
AWI-ESM-1-1-LR	Alfred Wegener Institute (AWI), Germany	1.875 x 1.865	Danek et al. 2020
CESM2-WACCM	National Center for Atmospheric Research (NCAR), United States	1.25 x 0.95	Danabasoglu (2019a)
CESM2		1.25 x 0.95	Danabasoglu (2019b)
CMCC-CM2-HR4	Fondazione Centro Euro-Mediterraneo sui Cambiamenti Climatici, Italy	1.25 x 0.95	Scoccimarro et al. (2020)
CMCC-CM2-SR5		1.25 x 0.95	Lovato and Peano (2020)
CMCC-ESM2		1.25 x 0.95	Lovato et al (2021)
EC-Earth3-AerChem	EC-Earth Consortium, Sweden	0.70 x 0.70	EC-Earth (2020a)
EC-Earth3-CC		0.70 x 0.70	EC-Earth (2021)
EC-Earth3-Veg-LR		1.125 x 1.121	EC-Earth (2020b)
EC-Earth3		0.70 x 0.70	EC-Earth (2019)
FGOALS-f3-L	Institute of Atmospheric Physics, Chinese Academy of Sciences (IAP, CAS), China	1.25 x 0.95	Yu (2019)
GFDL-CM4	Geophysical Fluid Dynamics Laboratory, National Oceanic and Atmospheric Administration (GFDL, NOAA), United States	1.25 x 1.00	Guo et al. (2018)
IPSL-CM6A-LR-INCA	Institute Pierre Simon Laplace (IPSL), France	2.50 x 1.27	Boucher et al. (2021)
IPSL-CM6A-LR		2.50 x 1.27	Boucher et al. (2018)
MIROC6	Japan Agency for Marine-Earth Science and Technology (JAMSTEC), Japan	1.4 x 1.4	Tatebe and Watanabe (2018)
MPI-ESM-1-2-HAM	Max Planck Institute für Meteorology (MPI), Germany	1.875 x 1.865	Neubauer et al. (2019)
MPI-ESM1-2-HR		0.94 x 0.94	Jungclaus et al. (2019)
MPI-ESM1-2-LR		1.875 x 1.865	Wieners et al. (2019)
MRI-ESM2-0	Meteorological Research Institute, Japan Meteorological Agency (MIR, JAM), Japan	1.125 x 1.121	Yukimoto et al. (2019)
NorCPM1	Norwegian Climate Centre (NCC), Norway	2.50 x 1.89	Bethke et al. (2019)
NorESM2-MM		1.25 x 0.94	Bentsen et al. (2019)
SAM0-UNICON	Seoul National University, South Korea	1.25 x 0.94	Park and Shin (2019)